CHEMISTRY OF MATERIALS
Article

*Chem. Mater.* **2009,** *21,* 4653–4660 4653
DOI:10.1021/cm901766y

# High Temperature Thermoelectric Response of Electron-Doped $CaMnO_3$

Yang Wang,[†,§] Yu Sui,*[,†,‡] Hongjin Fan,[§] Xianjie Wang,[†] Yantao Su,[†] Wenhui Su,[†] and Xiaoyang Liu[∥]

[†]*Center for Condensed Matter Science and Technology (CCMST), Department of Physics, Harbin Institute of Technology, Harbin 150001, People's Republic of China,* [‡]*International Center for Materials Physics, Academia Sinica, Shenyang 110015, People's Republic of China,* [§]*Division of Physics, Applied Physics, School of Physical and Mathematical Sciences, Nanyang Technological University, 21 Nanyang Link, 637371, Singapore, and*[∥] *State Key Laboratory of Inorganic Synthesis and Preparative Chemistry, College of Chemistry, Jilin University, 2699 Qianjin Street, Changchun 130012, People's Republic of China*

*Received June 24, 2009. Revised Manuscript Received September 2, 2009*

We report a systematical investigation on the high temperature thermoelectric response of $Ca_{1-x}R_xMnO_3$ (R = rare-earth) perovskites in the electron-doped range. The results reveal that electron concentration is the dominant factor for the high temperature electrical transport properties whereas the weight and size of R ions dominate the thermal transport properties. As the doping level varies, the best thermoelectric performance is observed at the relative electron concentration around 0.1. However, in the case of a fixed electron concentration, structural distortions become important since bandwidth has an observable influence on resistivity. By combining the three factors, electron concentration, crystal structure, and the weight/size of R ions, the largest thermoelectric figure of merit $ZT$ for $Ca_{1-x}R_xMnO_3$ reaches 0.2 at 1000 K. But this $ZT$ value is still too far from the application criterion ($ZT > 1$). Using the dynamical mean field theory, we demonstrate that a $ZT$ value larger than one in electron-doped $CaMnO_3$ systems seems rather unlikely. Some strategies for searching new thermoelectric materials with high performance in transition metal oxides are proposed.

## Introduction

Thermoelectric (TE) materials and thermoelectric effects, which are responsible for the direct conversion of heat into electrical energy and vice versa, have attracted much attention recently driven by their application as clean energy sources and device coolers.[1,2] The energy conversion performance of a TE material is usually evaluated by the dimensionless figure of merit $ZT = S^2T/\rho\kappa$, where $S$, $\rho$, and $\kappa$ are thermopower, resistivity, and thermal conductivity, respectively. For practical applications, it is necessary that $ZT > 1$, which requires a larger $S$ but lower $\rho$ and $\kappa$. However, these three parameters are not independent but instead all depend on carrier concentration. For example, $S$ will dramatically increase as the carrier concentration decreases, but simultaneously $\rho$ is also enhanced. Accordingly, the optimum carrier concentration is estimated to be $\sim 10^{19}$ cm$^{-3}$.[3] On the basis of this restriction, to date only a few intermetallic compound semiconductors such as $Bi_2Te_3$ alloys, chalcogenides, and skutterudites are known to fulfill the requirement,[3−5] and these TE alloys remain the state-of-the-art high $ZT$ materials even today.

Compared with the above conventional TE alloys, metal oxides are more suitable for high temperature applications because of their structural and chemical stabilities, oxidation resistance, easy manufacture, and low cost. But for metal oxides, the strong ionic character with narrow conduction bandwidths arising from weak orbital overlap usually leads to the localization of electrons with low carrier mobilities, which therefore gives rise to poor TE performance.[6,7] That is why metal oxides have been avoided in the search for good TE materials for a long time. However, some 3d transition metal oxides, such as titanates, cobaltites, and manganites, have received renewed attention recently as a new category of TE materials because the pronounced TE response was observed in these compounds.[8−13] The carrier concentration

*Corresponding author. E-mail: suiyu@hit.edu.cn.

(1) Mahan, G. D. *Solid State Phys.* **1998**, *51*, 81.
(2) Bell, L. E. *Science* **2008**, *321*, 1457.
(3) Snyder, G. J.; Toberer, E. S. *Nat. Mater.* **2008**, *7*, 105.
(4) Xiao, F.; Hangarter, C.; Yoo, B.; Rheem, Y.; Lee, K. H.; Myung, N. V. *Electrochim. Acta* **2008**, *53*, 8103.
(5) Minnich, A. J.; Dresselhaus, M. S.; Ren, Z. F.; Chen, G. *Energy Environ. Sci.* **2009**, *2*, 466.
(6) Sales, B. C.; Mandrus, D. G.; Chakoumakos, B. C. In *Recent trends in thermoelectric materials research II*; Tritt, T., Ed.; Academic Press: New York, 2001.
(7) He, T.; Chen, J. Z.; Calvarese, T. G.; Subramanian, M. A. *Solid State Sci.* **2006**, *8*, 467.
(8) Ohta, H.; Sugiura, K.; Koumoto, K. *Inorg. Chem.* **2008**, *47*, 8429.
(9) Ohta, H.; Kim, S.; Mune, Y.; Mizoguchi, T.; Nomura, K.; Ohta, S.; Nomura, T.; Nakanishi, Y.; Ikuhara, Y.; Nirano, M.; Nosono, H.; Koumoto, K. *Nat. Mater.* **2007**, *6*, 129.
(10) Ohtaki, M.; Koga, H.; Tokunaga, T.; Eguchi, K.; Arai, H. *J. Solid State Chem.* **1995**, *120*, 105.
(11) Okuda, T.; Nakanishi, K.; Miyasaka, S.; Tokura, Y. *Phys. Rev. B* **2001**, *63*, 113104.
(12) Androulakis, J.; Migiakis, P.; Giapintzakis, J. *Appl. Phys. Lett.* **2004**, *84*, 1099.
(13) Masset, A. C.; Michel, C.; Maignan, A.; Hervieu, M.; Toulemonde, O.; Studer, F.; Raveau, B.; Hejtmanek, J. *Phys. Rev. B* **2000**, *62*, 166.


Published on Web 09/21/2009

of these metal oxides can reach $\sim 10^{21}$ cm$^{-3}$, but these compounds yet show a thermopower comparable to that of the traditional low-carrier-concentration TE alloys. Among these metal oxides, mixed-valent manganite perovskites show complex electrical, magnetic, and thermal properties.[14,15] In addition to these rich properties, electron-doped manganites also exhibit good TE performance owing to their relatively larger thermopower and lower resistivity.[10,16] Just so, some all-oxides TE power generator modules have been fabricated with electron-doped $CaMnO_3$ as *n*-type legs.[17] However, the thermoelectric properties of electron-doped manganites are still low compared with *p*-type TE cobalt oxides, which leads to the mismatching and thus poor output power. In fact, compared with excellent *p*-type TE oxides such as layered cobaltites of which $ZT$ can reach 1.2−2.7 above 873 K,[18] good *n*-type TE oxides with high $ZT$ are very scanty. To our knowledge, $ZT \sim 0.37$ at 1000 K of Nb-doped $SrTiO_3$ is the largest value among *n*-type oxides ever reported.[19] For a TE device, high-performance *n*-type and *p*-type materials are both indispensable, so the search of good *n*-type TE oxides is prerequisite to applicable all-oxide TE devices at present.

To overcome the disadvantage of *n*-type oxides and get better *n*-type TE materials, many attempts have been made to improve the TE performance of electron-doped manganites by choosing various kinds of doped ions,[10,16,20−24] and the $ZT$ of this family is indeed enhanced by these investigations. Nevertheless, the optimal $ZT$ values of the manganites obtained from these investigations are all between $10^{-2}$−$10^{-1}$ order of magnitude, thus still far from the applications. In addition, although the effects of electron-doping by different ions on high temperature TE properties of manganites are similar, a quantitative relation of carrier concentration, bandwidth, crystal structure, and so forth with the TE properties remains unexplored, while the investigation on this aspect is essential to understand the source of the TE response in these manganite perovskites. Therefore, systematical and detailed study is highly needed to clarify the relationship between TE properties and doped ions. Most importantly, based on the fact that large numbers of investigations on the electron-doped manganites were reported but $ZT \sim 10^{-1}$ order of magnitude at most, it is also required to explore whether a $ZT$ larger than one can be reached in this system and how to achieve it. Such a study may also shed light on the ongoing search for new TE materials.

In this study, we prepared a series of rare-earth doped $CaMnO_3$ for a systematical investigation of their high temperature TE properties. Skipping the details of phase diagram and magnetic properties of electron-doped $CaMnO_3$ system, we focus on the transport properties relative to thermoelectricity, to explore the factors that determine the high temperature TE response and the possible largest $ZT$ of this family.

## Experimental Section

$Ca_{1-x}R_xMnO_3$ ($x = 0$−0.2, R = La, Ce, Pr, Nd, Sm, Eu, Gd, Tb, Dy, Ho, Er, Yb, and Y) ceramics were prepared by conventional solid-state reaction. First, stoichiometric amounts of $CaCO_3$, $MnO_2$, $La_2O_3$, $CeO_2$, $Pr_6O_{11}$, $Sm_2O_3$, $Eu_2O_3$, $Gd_2O_3$, $Tb_4O_7$, $Dy_2O_3$, $Ho_2O_3$, $Er_2O_3$, $Yb_2O_3$, and $Y_2O_3$ powders were mixed and calcined at 1273 K for 12 h. The mixture was then ground, pressed into pellets, and sintered at 1573 K for 24 h. Finally, the products were reground thoroughly and pressed into pellets again, followed by sintering at 1623 K for 36 h. The pellets were slowly cooled to room temperature in the furnace. All the calcination processes were conducted in air.

X-ray diffraction (XRD) data at room temperature were carried out by using a Bede $D^1$ XRD diffractometer with Ni filtered Cu K$\alpha$ ($\lambda = 0.15406$ nm) radiation. The XRD data confirm that all the samples are assigned to be single-phase of the orthorhombic-perovskite structure describing by the *Pnma* space group. Detailed structural parameters determined by Rietveld refinement were reported elsewhere.[25,26] The microstructure was observed with a JEOL JSM-6700F scanning electron microscope (SEM). The SEM micrographs indicate that these ceramics are quite dense and without obvious pores. The typical grain size is $\sim 3-5$ $\mu$m. The density $d$ (measured by the Archimedes method at room temperature) of all the samples is $\sim 4.3$ g/cm$^3$ (except for Y doped specimens, $d \sim 4.1-4.2$ g/cm$^3$). Detailed density data and SEM micrographs of selected samples are shown in Supporting Information. Iodometic titration indicated that the oxygen content of all specimens fell within the range $3.00 \pm 0.01$. Thermogravimetric analysis (TGA), measured by SDT 2960 of TA Instruments, was used to check the oxygen stoichiometry and the average valence of Mn.

Resistivity from room temperature to 1073 K was measured by a standard four-probe method, using 2400 SourceMeter (Keithley). Silver leads were attached to four points on the top surface of the bar-shaped samples (with typical size of 10 mm × 1 mm × 1 mm), with silver paste that served as electrodes. Thermopower from 300 K to 1000 K was calculated from the temperature gradient $\Delta T$ across the samples and the thermoelectric voltage $\Delta V$ collected with 2000 Multimeter (Keithley). One end of the bar-shape sample was heated to produce a temperature difference between both ends of the sample up to 5 K, when the $\Delta V$ and $\Delta T$ were simultaneously measured. Then thermopower $S$ was obtained by the slop of $\Delta V/\Delta T$ calculated from more than 50 pairs of $\Delta V$ and $\Delta T$ at each measured

(14) Siwach, P. K.; Singh, H. K.; Srivastava, O. N. *J. Phys.: Condens. Matter* **2008**, *20*, 273201.
(15) Phan, M. H.; Yu, S. C. *J. Magn. Magn. Mater*. **2007**, *308*, 325.
(16) Flahaut, D.; Mihara, T.; Funahashi, R.; Nabeshima, N.; Lee, K.; Ohta, H.; Koumoto, K. *J. Appl. Phys*. **2006**, *100*, 084911.
(17) Matsubara, I.; Funahashi, R.; Takeuchi, T.; Sodeoka, S.; Shimizu, T.; Ueno, K. *Appl. Phys. Lett*. **2001**, *78*, 3627. Reddy, E. S.; Noudem, J. G.; Hébert, S.; Goupil, C. *J. Phys. D: Appl. Phys* **2005**, *38*, 3751.
(18) Funahashi, R.; Matsubara, I.; Ikuta, H.; Takeuchi, T.; Mizutani, U.; Sodeoka, S. *Jpn. J. Appl. Phys*. **2000**, *39*(Part 2), L1127.
(19) Ohta, S.; Nomura, T.; Ohta, H.; Hirano, M.; Hosono, H.; Koumoto, K. *Appl. Phys. Lett*. **2005**, *87*, 1092108.
(20) Cong, B. T.; Tsuji, T.; Thao, P. X.; Thanh, P. Q.; Yamamura, Y. *Physica B* **2004**, *352*, 18.
(21) Xu, G. J.; Funahashi, R.; Pu, Q. R.; Liu, B.; Tao, R. H.; Wang, G. S.; Ding, Z. J. *Solid State Ionics* **2004**, *171*, 147. Xu, G. J.; Funahashi, R.; Matsubara, I.; Shikano, M.; Zhou, Y. Q. *J. Mater. Res*. **2002**, *17*, 1092.
(22) Wang, Y.; Sui, Y.; Su, W. H. *J. Appl. Phys*. **2008**, *104*, 093703.
(23) Wang, Y.; Sui, Y.; Wang, X. J.; Su, W. H. *J. Phys. D: Appl. Phys*. **2009**, *42*, 055010.
(24) Maignan, A.; Hébert, S.; Pi, L.; Pelloquin, D.; Martin, C.; Michel, C.; Hervieu, M.; Raveau, B. *Cryst. Eng*. **2002**, *5*, 365.
(25) Wang, Y.; Sui, Y.; Cheng, J. G.; Wang, X. J.; Lu, Z.; Su, W. H. *J. Phys. Chem. C* **2009**, *113*, 12509.
(26) Wang, Y.; Sui, Y.; Wang, X. J.; Su, W. H. *J. Phys.: Condens. Matter* **2009**, *21*, 196004.

temperature. Also, silver leads were used for thermoelectric voltage record. Both resistivity and thermopower measurements were performed in air and ambient pressure. Thermal conductivity $\kappa$ was calculated by $\kappa = DC_p d$, where $D$ is thermal diffusivity (measured by a laser flash method, Netzsch LFA-427), $C_p$ is specific heat capacity (determined by Netzsch DSC 404), and $d$ is material density. One face of the disk-shaped sample was irradiated by a short (<1 ms) laser pulse, and an infrared detector monitored the temperature rise of the opposite side of the sample. Then $D$ was determined from the temperature rise versus time profile. $C_p$ was determined by differential scanning calorimetry (DSC). The powder samples were heated from room temperature to 1000 K; the temperature scan rate was controlled at 5 K/min. All these thermal measurements were performed in a vacuum. A systematic error up to 10% of thermal conductivity measurements cannot be avoided in this study.

## Results and Discussion

Figure 1 presents temperature dependence of resistivity $\rho$, thermopower $S$, and power factor $P$ (defined by $P = S^2/\rho$) from room temperature to 1000 K for four representative sets of samples. Other samples have similar behavior. Compared with semiconducting-like $CaMnO_3$ whose resistivity is on the order of magnitude $\sim 10^3$ m$\Omega$ cm,[27] doping at the Ca-site with rare-earth ions significantly lowers $\rho$. The behavior of $\rho(T)$ also gradually changes; some samples exhibit metallic-like transport behavior at elevated temperatures. With increasing doping level, $\rho$ values first decrease, with minima around $x \sim 0.1-0.12$, and then increase. The reduction of $\rho$ at first should be attributed to the enhancement of electron concentration by trivalent $R^{3+}$ doping. On the basis of valence equilibrium, the substitution of $R^{3+}$ for $Ca^{2+}$ will add $Mn^{3+}$ ions, create large numbers of electron carriers, and thus facilitate the electron hopping between $Mn^{3+}$ and $Mn^{4+}$ sites and then decrease $\rho$ as a result.[28,29] However, in the electron-doped $CaMnO_3$ system, when the electron concentration exceeds a certain magnitude (corresponding to $x \sim 0.1-0.12$), charge ordering or local charge ordering arises.[26,27,30−32] Since charge ordering can result in the localization of electrons, $\rho$ of a system will be enhanced when charge ordering occurs. Therefore, the doping level dependence of $\rho$ values is not monotonous; the minimum of resistivity exists just before the onset of charge ordering state.

In contrast to resistivity, thermopower has a monotonous dependence on doping level in this system (see the middle row in Figure 1). As the electron concentration increases, the absolute value $|S|$ monotonously decreases. Limited by Heikes's rule,[33] thermopower is in inverse of the electron concentration roughly at high temperature, so $|S|$ will decrease with the enhancement of doping level since more electrons are introduced. In this regard, one can see that the high temperature resistivity and thermopower behaviors are mainly determined by the electron concentrations in this system. In other words, if two $Ca_{1-x}R_xMnO_3$ samples have the same $R^{3+}$ content, they will show almost the same $\rho$ and $S$.

Using the measured values of $\rho$ and $S$, the temperature dependence of power factor $P$ can also be plotted. As seen from the bottom row in Figure 1, larger $P$ values appear only in the electron concentration range of 0.06−0.12, due to relatively lower $\rho$ and moderate $S$ in these samples. Since the samples in such an electron concentration range exhibit larger $P$, their thermal conductivity $\kappa$ is measured and $ZT$ values are calculated, as shown in Figure 2. The values of $\kappa$ lower with the increase of doping level for each R-doped series specimens. $\kappa$ in the paramagnetic range (all $Ca_{1-x}R_xMnO_3$ series are paramagnetic above room temperature) can be expressed by the sum of phonon thermal conductivity term $\kappa_{ph}$ and electron carrier thermal conductivity term $\kappa_{ele}$, namely, $\kappa = \kappa_{ph} + \kappa_{ele}$. According to Wiedemann−Franz's law, $\kappa_{ele} = L_0 T/\rho$, where $L_0 = \pi^2 k_B^2/3e^2 = 2.45 \times 10^{-8}$ W $\Omega$ K$^{-2}$ is the Lorentz constant. From the calculated results of $\kappa_{ph}$ and $\kappa_{ele}$ (see the middle row of Figure 2), the contribution of $\kappa_{ele}$ to total $\kappa$ is small (the largest percentage of $\kappa_{ele}$ is less than 15%), so $\kappa_{ph}$ is the predominant component in $\kappa$ of the system. Therefore, the variation of $\kappa$ mainly originates from the change in $\kappa_{ph}$. Considering the large mass difference and size mismatch between R and Ca, as the content of R ions increases, the mass disorder and crystal structural distortions enhance so that the increasing unharmonious lattice vibration can markedly suppress the phonon transport. Consequentially, $\kappa$ will decrease with doping. Therefore, s$\kappa$ of this system is mainly dependent on the radius and weight of the doped ion rather than the electron concentration.

A special case of $Ce^{4+}$ doped samples can be used to further verify the above conclusions on electrical and thermal transport, in virtue of the tetravalent characteristic of $Ce^{4+}$ ion. All the TE parameters of $Ce^{4+}$ doped samples are plotted versus temperature in Figure 3, from which it can be found that the TE response of $Ce^{4+}$ doped samples is similar with that of $R^{3+}$ doped samples. More importantly, from Figures 1−3, one can find the magnitudes of $\rho$ and $S$ of $Ce^{4+}$ doped samples are consistent with those of $R^{3+}$ doped samples, provided that the $Ce^{4+}$ content is half of the $R^{3+}$ content. On the other hand, the magnitudes of $\kappa$ of $Ce^{4+}$ doped samples are comparable to those of $R^{3+}$ doped samples in the case that $Ce^{4+}$ and $R^{3+}$ have the same level. This comparison unambiguously demonstrates that the electron concentration dominates $\rho$ and $S$ whereas the radius and weight of doped ion dominate $\kappa$.

Combining $\rho$, $S$, and $\kappa$, $ZT$ values of these samples are calculated. From the bottom row in Figure 2 (and the $ZT$ of Ce doped specimens in Figure 3), it appears that the $ZT$ values of each series are not larger than 0.2. As the highest

(27) Melo Jorge, M. E.; Nunes, M. R.; Silva Maria, R.; Sousa, D. *Chem. Mater.* **2005**, *17*, 2069.
(28) Jakob, G.; Westerburg, W.; Martain, F.; Adrian, H. *Phys. Rev. B* **1998**, *58*, 14966.
(29) Chun, S. H.; Salamon, M. B.; Lyanda-Geller, Y.; Goldbart, P. M.; Han, P. D. *Phys. Rev. Lett.* **2000**, *84*, 757.
(30) Raveau, B.; Maignan, A.; Martin, C.; Hervieu, M. *Chem. Mater.* **1998**, *10*, 2641.
(31) Sudheendra, L.; Raju, A. R.; Rao, C. N. R. *J. Phys: Condens. Matter* **2003**, *15*, 895.
(32) Caspi, E. N.; Avdeev, M.; Short, S.; Jorgensen, J. D.; Lobanov, M. V.; Zeng, Z.; Greenblatt, M.; Thiyagarajan, P.; Botez, C. E.; Stephens, P. W. *Phys. Rev. B* **2004**, *69*, 104402.
(33) Heikes, R. P. In *Transition Metal Compounds*; Schatz, E. R., Ed.; Gordon and Breach: New York, 1963.

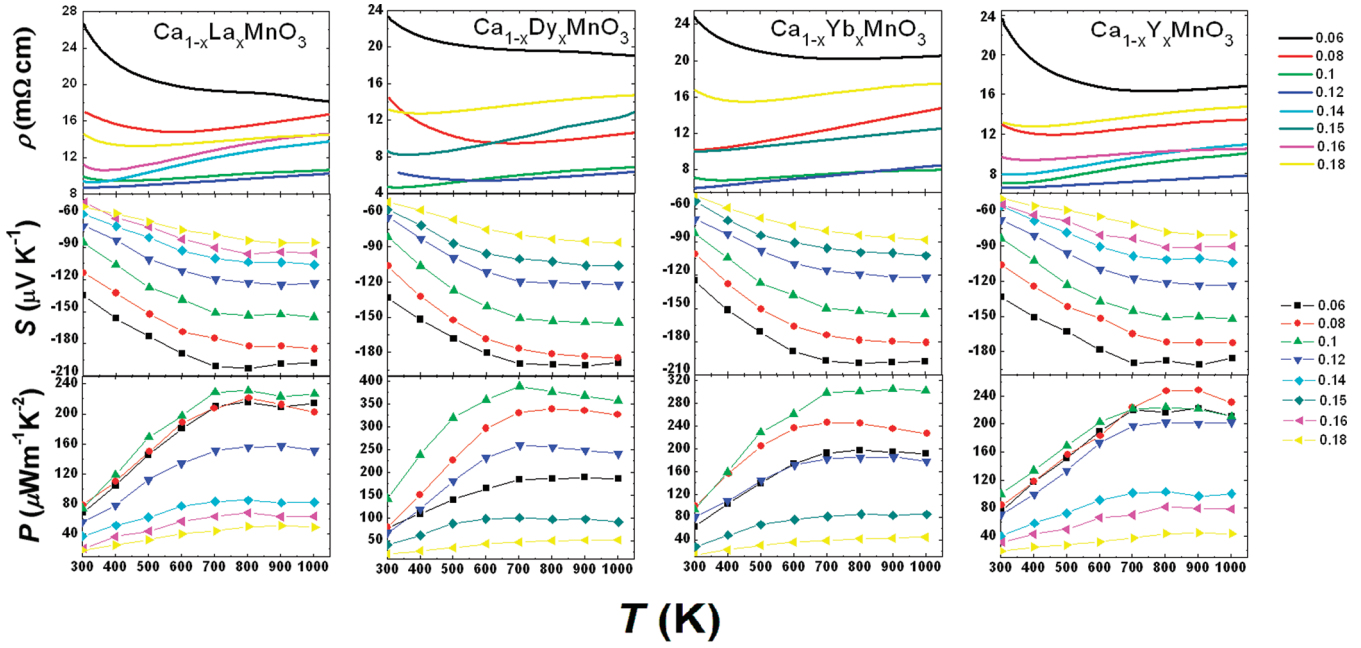


**Figure 1.** Temperature dependence of resistivity $\rho$, thermopower $S$, and power factor $P$ for $Ca_{1-x}R_xMnO_3$ (R = La, Dy, Yb, and Y) samples.

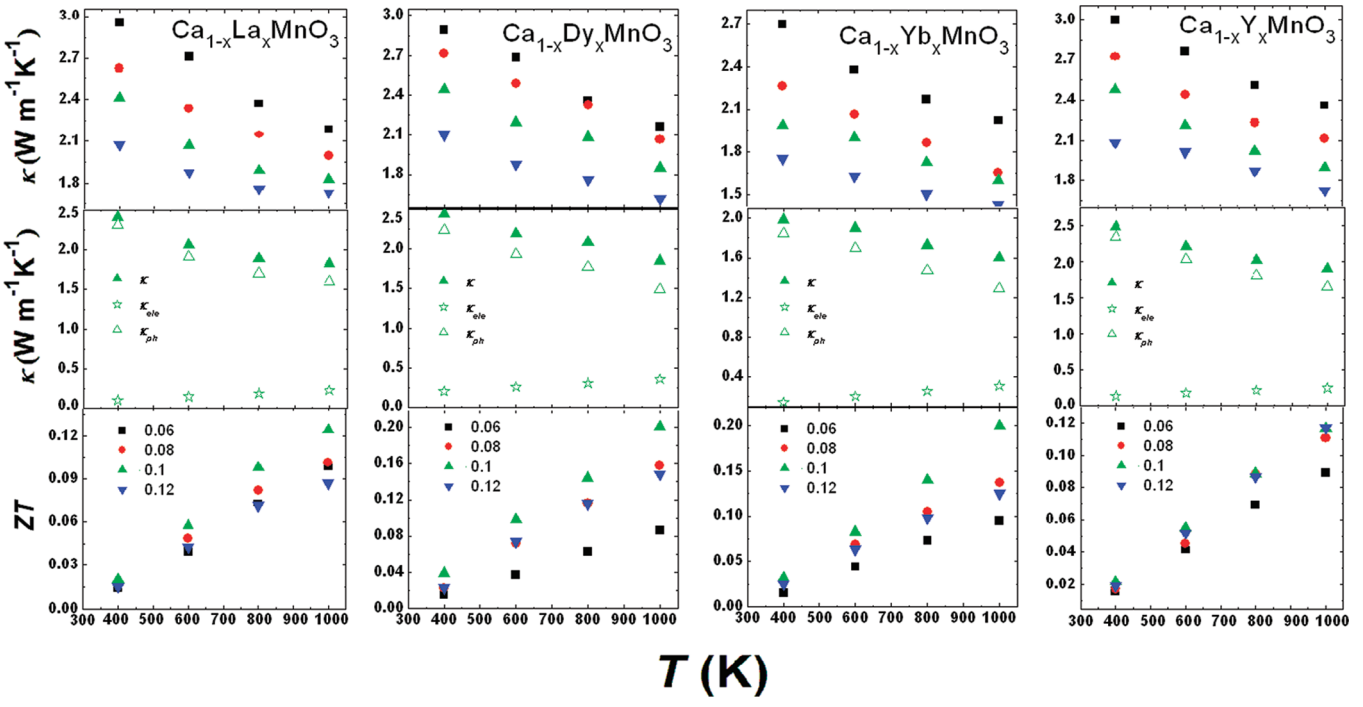


**Figure 2.** Temperature dependence of thermal conductivity $\kappa$ and figure of merit $ZT$ for $Ca_{1-x}R_xMnO_3$ (R = La, Dy, Yb, and Y) samples. The middle row gives total thermal conductivity $\kappa$, phonon thermal conductivity $\kappa_{ph}$, and electron carrier thermal conductivity $\kappa_{ele}$ for the $x = 0.1$ samples of these four series.

$ZT$ of this system always occurs at the doping level $x = 0.1$ (for $Ce^{4+}$ doped series, $x = 0.05$), next we focus on the $Ca_{0.9}R_{0.1}MnO_3$ samples to probe the possibility of further enhancement of $ZT$. Figure 4a collects $\rho(T)$ curves of $Ca_{0.9}R_{0.1}MnO_3$. Apparently, $Ca_{0.9}R_{0.1}MnO_3$ exhibit different resistivity even if they have the same electron concentration. Because electrical conduction in manganites is governed by $e_g$ electrons, we have to consider the effective $e_g$ bandwidth $W$ that is determined by structural parameters. In orthorhombic perovskites, $W \propto \cos\omega/d_{Mn-O}^{3.5}$ within the tight-binding approximation, where $\omega = (\pi - \theta_{Mn-O-Mn})/2$, $\theta_{Mn-O-Mn}$ and $d_{Mn-O}$ denote the average Mn−O−Mn bond angle and Mn−O bond length, respectively.[34] The calculated relative bandwidth $W_r$ ($= W_{Ca_{0.9}R_{0.1}MnO_3}/W_{Ca_{0.9}La_{0.1}MnO_3}$) is shown in Figure 4b, in which the resistivity at room temperature ($\rho_{RT}$) and 1000 K ($\rho_{1000K}$) and the power factor at

(34) Medarde, M.; Mesot, J.; Lacorre, P.; Rosenkranz, S.; Fischer, P.; Gobrecht, K. *Phys. Rev. B* **1995**, *52*, 9248.

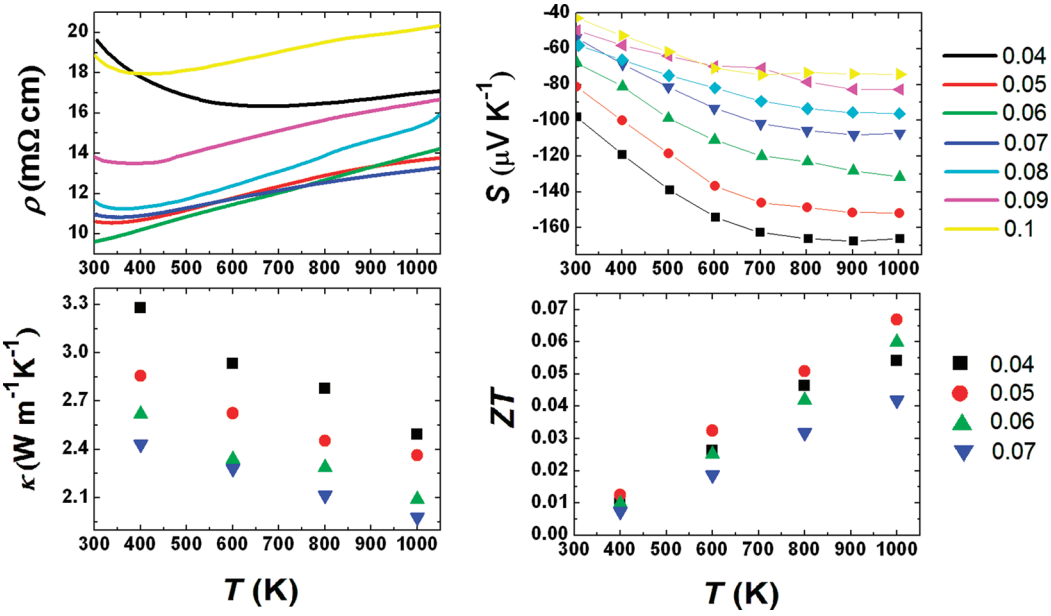


**Figure 3.** Temperature dependence of $\rho$, $S$, $\kappa$, and $ZT$ of $Ca_{1-x}Ce_xMnO_3$.

1000 K ($P_{1000K}$) as a function of the average $A$-site ionic radius $\langle r_A \rangle$ are also presented. It can be seen that the bandwidth and resistivity exhibit an opposite evolution as $\langle r_A \rangle$ decreases from La to Yb. This is within expectation as the hopping of $e_g$ electrons underlies the electrical conduction and the enhanced effective bandwidth of $e_g$ electron will lower resistivity accordingly. $Ca_{0.9}Dy_{0.1}MnO_3$ exhibits a largest $W_r$, corresponding to its lowest resistivity. Therefore, we can conclude that the slight difference of bandwidth induced by structural distortions gives rise to the different resistivities in this system, even though these samples have equal electron concentrations. Furthermore, similar to resistivity, the metal−insulator transition temperature $T_{MI}$ (defined as the temperature that $d\rho/dT = 0$ in $\rho(T)$ curves) also shows such an evolution with $\langle r_A \rangle$, suggesting the correlation between crystal structure and electrical transport properties. The special case is the Y doped sample. Because the Y doped sample has relatively lower density and more pores in the microstructure than all the others (see Supporting Information), it exhibits a higher resistivity than that of the Ho doped sample even if they have nearly identical $\langle r_A \rangle$ and bandwidth. Nevertheless, $T_{MI}$ is almost same for Y and Ho doped samples, revealing that structure and bandwidth indeed have an intrinsic correlation to electrical transport properties.

Different from resistivity, thermopower of the samples does not exhibit any observable difference from room temperature to 1000 K (see Figure 5). This result indicates that $S$ is not sensitive to crystal structure factor and crystallographic defects but only determined by electron concentration. Although structural distortions can observably influence $\rho$, they have less effect on $S$. In this case, as shown in the bottom row of Figure 4b, $P$ of this family behaves oppositely to $\rho$ with $\langle r_A \rangle$ alteration and shows a peak value at $Ca_{0.9}Dy_{0.1}MnO_3$. $P$ at 1000 K can reach 360 $\mu$W m$^{-1}$ K$^{-2}$, which is quite high among $n$-type TE oxides.

Figure 6a shows thermal conductivity at room temperature ($\kappa_{RT}$) and 1000 K ($\kappa_{1000K}$) as a function of $\langle r_A \rangle$. With decreasing $\langle r_A \rangle$, thermal conductivity keeps almost unchanged from La to Nd but decreases gradually from Sm to Yb. Due to the dominant role of $\kappa_{ph}$ in thermal conductivity, the variation of $\kappa$ from La to Yb also arises from the change in $\kappa_{ph}$. Actually, the effects of R doping on phonon transport involve two aspects: one is the crystallographic distortions caused by the substitution of R for Ca; the other, which is usually more important to thermal conductivity, is that the weight of R is much heavier than Ca.[16] Due to the large weight difference between R and Ca, R ions can vibrate independently from the other ions (viz. local vibration). As a result, the mean free path of phonons will be shortened, and thus $\kappa_{ph}$ will be suppressed. In this context, more weight difference between R and Ca will lead to more reduction of $\kappa_{ph}$, so a gradual decrease in thermal conductivity can be anticipated as R varies from La to Yb. It should be noted that in the samples with smaller $\langle r_A \rangle$ the noticeable structural distortions also play a role in the suppression of $\kappa$. The weight of Y is much lighter than La, but $\kappa$ of $Ca_{0.9}Y_{0.1}MnO_3$ is comparable with that of $Ca_{0.9}La_{0.1}MnO_3$, just due to the stronger distortion in $Ca_{0.9}Y_{0.1}MnO_3$. Similarly, Ce is nearly as heavy as La, but $Ca_{0.9}Ce_{0.1}MnO_3$ has observably lower $\kappa$ than $Ca_{0.9}La_{0.1}MnO_3$, also because of the larger distortion in $Ca_{0.9}Ce_{0.1}MnO_3$. In a word, the weight and size of R both play roles in the reduction of $\kappa$ in this family.

After adding the factor of thermal conductivity to the power factor, as can be seen from Figure 6b, $Ca_{0.9}Yb_{0.1}MnO_3$ and $Ca_{0.9}Dy_{0.1}MnO_3$ have the highest $ZT$ value concurrently. This is mainly on account of the lowest $\kappa$ of $Ca_{0.9}Yb_{0.1}MnO_3$.

On the basis of the above experimental results, we see that $S$ is determined only by electron concentration (i.e., doping level); $\rho$ relies on both electron concentration and

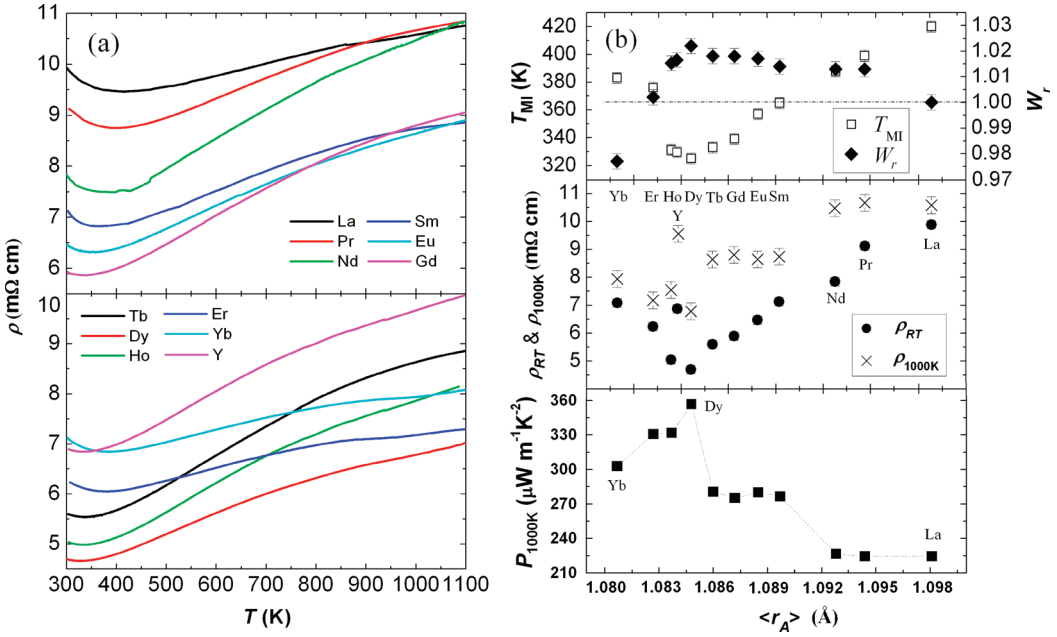


**Figure 4.** (a) Temperature dependence of $\rho$ for $Ca_{0.9}R_{0.1}MnO_3$ samples; (b) metal−insulator transition temperature $T_{MI}$, relative effective $e_g$ bandwidth $W_r$, room-temperature resistivity $\rho_{RT}$, 1000 K resistivity $\rho_{1000K}$, and 1000 K power factor $P_{1000K}$ as a function of average A-site ionic radius $\langle r_A \rangle$ for $Ca_{0.9}R_{0.1}MnO_3$ samples.

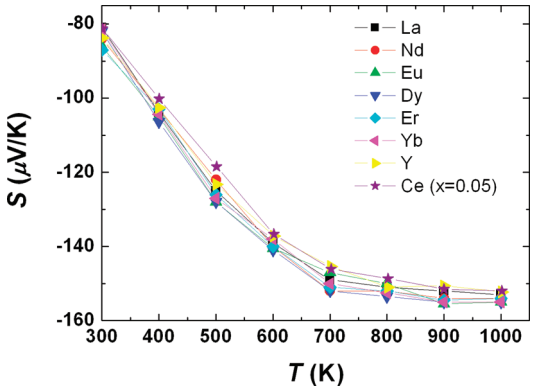


**Figure 5.** Temperature dependence of $S$ for $Ca_{0.9}R_{0.1}MnO_3$ samples ($S$ of $Ca_{0.95}Ce_{0.05}MnO_3$ is also shown).

crystal structure factor, while $\kappa$ is dominated by the weight and size of doped ions. When these three factors (electron concentration, crystal structure, and the weight/size of R ion) are combined, we obtain the optimal $ZT$ in $Ca_{1-x}R_xMnO_3$ system to be 0.2 at 1000 K. Although this $ZT$ value is rather large among $n$-type oxides, it is still too low compared to the applied criterion ($ZT > 1$). So after the systematic experimental investigations on these rare-earth doped $CaMnO_3$, we come to a point to ask what is the largest $ZT$ that $Ca_{1-x}R_xMnO_3$ can reach and whether $ZT > 1$ can be achieved in this family.

According to the dynamical mean field theory,[35−38] resistivity $\rho$, thermopower $S$, and electron thermal conductivity $\kappa_{ele}$ at the high temperature limit in electronic systems can be described as

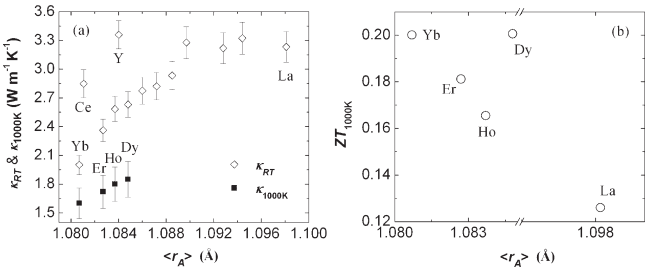


**Figure 6.** (a) Room-temperature thermal conductivity $\kappa_{RT}$ and 1000 K thermal conductivity $\kappa_{1000K}$; (b) $ZT$ values at 1000 K $ZT_{1000K}$ as a function of $\langle r_A \rangle$ for $Ca_{0.9}R_{0.1}MnO_3$ samples.

$$\rho = \left(\frac{\alpha\hbar}{e^2}\right)\frac{\frac{N}{x(1-x)}\left[\frac{x}{N}+(1-x)\right]^2}{\pi N(W\beta)\gamma_1} \quad (1)$$

$$S = \frac{k_B}{e}\ln\left[\frac{x}{N(1-x)}\right] \quad (2)$$

$$\kappa_{ele} = \left(\frac{k_B W}{\alpha\hbar}\right)\frac{\pi N(W\beta)^2\gamma_2}{\frac{N}{x(1-x)}\left[\frac{x}{N}+(1-x)\right]^2} \quad (3)$$

where $x$ is electron concentration (viz. the content of $Mn^{3+}$), $N$ is degeneracy, $W$ is bandwidth, $\alpha$, $\gamma_1$, and $\gamma_2$ are coefficients, and $k_B$ and $\hbar$ are the Boltzmann constant and Plank constant, respectively.[38] $\beta$ is an energy correlated parameter, and $\beta \propto 1/T$. To make the calculation of $ZT$ feasible, we use the expression of $\beta$ in the high temperature regime as

$$\beta = \frac{1}{\mu}\ln\left[\frac{x}{N(1-x)}\right] \quad (4)$$

(35) Jarrell, M. *Phys. Rev. Lett.* **1992**, *69*, 168.
(36) Pruschke, T.; Jarrell, M.; Freericks, J. K. *Adv. Phys.* **1995**, *44*, 187.
(37) Georges, A.; Kotliar, G.; Krauth, W.; Rozenberg, M. J. *Rev. Mod. Phys.* **1996**, *68*, 13.
(38) Pálsson, G.; Kotliar, G. *Phys. Rev. Lett.* **1998**, *80*, 4775.
(39) Cohn, J. L.; Neumeier, J. J. *Phys. Rev. B* **2002**, *66*, 100404(R).

in which $\mu = \varepsilon_0 - k_B T \ln g$ denotes chemical potential.[37,38] Given the above expressions, the definition of $ZT$

$$ZT = \frac{S^2 T}{\rho\kappa} = \frac{S^2 T}{\rho(\kappa_{ph} + \kappa_{ele})} \quad (5)$$

can be written as

$$ZT \propto \frac{\pi\gamma'_1 \ln^2\left[\frac{x}{N(1-x)}\right] x(1-x)}{\kappa_{ph}\left(\frac{\alpha\hbar}{k_B W}\right) + \pi\gamma'_2 (W\beta)^2 x(1-x)} \quad (6)$$

at the high temperature limit, in which the $\gamma_n'$ values are constants whereas $\gamma_n = \gamma_n'(1 - x + x/N)^2$ $(n = 1, 2)$.[38] Equation 6 indicates that $ZT$ is a function of $x$, $W$, and $\kappa_{ph}$ in the case of the high temperature limit. For perovskite manganites, 1000 K is enough to be considered as the high temperature limit, because the electronic kinetic energy is much larger than the other energies (Jahn−Teller splitting, Coulomb interactions, etc.) at 1000 K. Therefore, eq 6 can be used to estimate $ZT$ at 1000 K of the present $Ca_{1-x}R_xMnO_3$ family. Generally speaking, $\kappa_{ph}$ reflects the behavior of phonon transport that has nothing to do with electron concentration. The investigations on thermal conductivity of this (Ca,R)$MnO_3$ family reported are very few,[20,39,40] but from these reports we find that the doping level dependence of phonon thermal conductivity in $Ca_{1-x}La_xMnO_3$ and $Ca_{1-x}Sm_xMnO_3$ at 300 K (refs 39 and 40) and $Ca_{1-x}Pr_xMnO_3$ at 1000 K (ref 20) can be described by exponential functions although the physical nature is not clear at this stage. Therefore, to remove the $\kappa_{ph}$ term from eq 6, we first fit the plot of $\kappa_{ph}$ of $Ca_{1-x}Pr_xMnO_3$ at 1000 K versus $x$ in a large doping range using an exponential function $\kappa_{ph1000K} = Ax^c$ (see Figure 7). The fitted parameters $A$ and $c$ are 1.19 and −0.15, respectively. As can be seen from Figure 7, the fitting curve is consistent with the $\kappa_{ph1000K}$ data of other R ions doped samples on the whole. Then in eq 6 we use this exponential function as an approximation to describe the values of $\kappa_{ph}$ at 1000 K. Now, $ZT$ is only determined by $x$ and $W$. We further assume that $W$ does not change with $x$ (this is a rough but reasonable assumption, since $W$ is determined by structural parameters viz. bond length and bond angle, which will not alter dramatically as $x$ varies); thus, $ZT$ becomes a function that only relates to $x$. Figure 8 presents the curve of $ZT$ versus $x$ according to eq 6 and the above considerations. One can find that with the increase of $x$, $ZT$ first rises sharply and then decreases smoothly; the peak value of $ZT$ occurs in the vicinity of $x = 0.08$, approximately consisting with the experimental results ($ZT$ peaks at $x = 0.1$). When we input the experimental data $x = 0.1$ and $ZT = 0.2$ to the equation $ZT = ZT(x)$, one can get the bandwidth $W \sim 0.12$ eV. On the other hand, if we assume $ZT$ of order unity can be reached and let $x = 0.08-0.1$ as well as $ZT = 1$ in eq 6, one will get the bandwidth $W \sim 0.005-0.008$ eV. However, as $W$ is determined by bond length and bond angle ($W \propto \cos\omega/d_{Mn-O}^{3.5}$), it is nearly

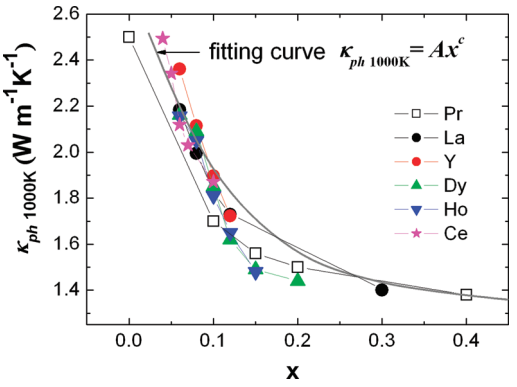


**Figure 7.** $\kappa_{ph1000K}$ of $Ca_{1-x}R_xMnO_3$ samples (the data of $Ca_{1-x}Pr_xMnO_3$ are from ref 20) and the exponential fitting curve $\kappa_{ph1000K} = Ax^c$.

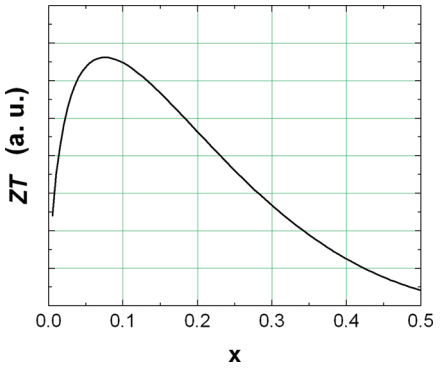


**Figure 8.** Curve of calculated $ZT$ as a function of $x$.

impossible to vary $W$ as large as 2 orders of magnitude through the change of structural distortions by ion doping (chemical pressure) or even high pressure. Therefore, in the light of our results, a $ZT$ value close to or larger than one in this family seems rather unlikely. This result may also explain why the highest $ZT$ obtained in electron-doped $CaMnO_3$ so far is still less than 0.2. Accordingly, it seems inadvisible to search applicable TE oxides among electron-doped manganite families, whether by choosing other ion doping or improving the prepared method.

Finally, we would like to propose some strategies in looking for new TE oxides among transition metal oxides. It has been considered that large electronic effective mass and spin/orbital degrees of freedom may be responsible for large thermopower in strongly correlated electron systems, where the former suggests stronger electronic correlation (narrower energy band) and the latter can cause large thermopower through degeneracy.[11,41−43] This means configurational entropy is a source of large thermopower in such strongly correlated systems such as cobaltites, and hence the transition metal oxides with rich spin/orbital degrees of freedom usually have good TE properties.[41,42] However, electron−phonon interaction, superexchange interaction, or double exchange interaction may also be strong in transition metal oxides, which

(40) Hejtmánek, J.; Jirák, Z.; Maryško, M.; Martin, C.; Maignan, A.; Hervieu, M.; Raveau, B. *Phys. Rev. B* **1999**, *60*, 14057.
(41) Koshibae, W.; Maekawa, S. *Phys. Rev. Lett.* **2001**, *87*, 236603.
(42) Wang, Y.; Rogado, N. S.; Cava, R. J.; Ong, N. P. *Nature* **2003**, *423*, 425.
(43) Limelette, P.; Hardy, V.; Auban-Senzier, P.; Jérome, D.; Flahaut, D.; Hébert, S.; Frésard, R.; Simon, Ch.; Noudem, J.; Maignan, A. *Phys. Rev. B* **2005**, *71*, 233108.

usually leads to a higher long-range ordering temperature (ferromagnetic transition temperature $T_C$, antiferromagnetic transition temperature $T_N$, orbital ordering temperature $T_{OO}$, etc.) in spin or orbital degrees of freedom. This will reduce entropy evidently and thus induce poor thermopower because there always exists short-range ordering in a large range above long-range ordering temperature. Hereby, lower ordering temperature is necessary for TE oxides. For the perovskite families, $T_C$, $T_N \propto W$ or $T_C$, $T_N \propto W^2$,[44] so we can see that the perovskite oxides with high thermopower should have larger bond length and/or smaller bond angle. On the other hand, the perovskites structure is usually considered as a "regular" structure and hence long-range ordering is easy to form. In contrast, the triangular lattice can prevent the long-range ordering; frustrated systems, such as spin/cluster glass, are also unfavorable to ordering, so they may be good candidates for TE oxides. For instance, $ZT$ values of layered cobaltites with triangular lattice can reach 0.8 or even larger than 1.2 around 1000 K,[18,45] and $La_{1-x}Sr_xCoO_3$ spin glass exhibits room-temperature $ZT$ as high as 0.18.[12] Actually, these characteristics are not incompatible. The strong electronic correlation implies large electronic effective mass and narrow band, while the small bond angle (pronounced deviation from 180°) usually leads to a small transfer integral and thus small bandwidth. This may also suggest the coupling between crystal structure and TE properties. Another way to improve TE performance is to effectively reduce thermal conductivity of materials. In addition to conventional methods such as doping heavy ions or enhancing structural distortions, orbital fluctuations can also significantly suppress the lattice contribution to thermal conductivity, as demonstrated in manganites and titanates.[46,47] Therefore, a system with complex orbital state may have not only a large thermopower but also a low thermal conductivity. This could be a new direction of searching good TE materials in transition metal oxides.

(44) Zhou, J. S.; Goodenough, J. B. *Phys. Rev. B* **2008**, *77*, 132104.
(45) Shikano, M.; Funahashi, R. *Appl. Phys. Lett.* **2003**, *82*, 1851.
(46) Zhou, J. S.; Goodenough, J. B. *Phys. Rev. B* **2001**, *64*, 024421.
(47) Cheng, J. G.; Sui, Y.; Zhou, J. S.; Goodenough, J. B.; Su, W. H. *Phys. Rev. Lett.* **2008**, *101*, 087205.

## Conclusion

In summary, we synthesized a series of $CaMnO_3$ electron-doped by rare-earth ions and systematically investigated their high temperature transport and thermoelectric properties. The results reveal that electron concentration, structural distortions, and the weight/size of doped ions are all related to the thermoelectric response of this system. Relatively large $ZT$ is exhibited in $Ca_{1-x}R_xMnO_3$ when $x$ equals 0.1 (for $Ca_{1-x}Ce_xMnO_3$, $x$ equals 0.05) on account of their low resistivity together with moderate thermopower. The highest $ZT$ is found in Dy and Yb doped samples among all $Ca_{0.9}R_{0.1}MnO_3$, attributed to the lowest resistivity and the lowest thermal conductivity of $Ca_{0.9}Dy_{0.1}MnO_3$ and $Ca_{0.9}Yb_{0.1}MnO_3$, respectively. Although the largest $ZT$ value 0.2 at 1000 K obtained in this study is quite high for $n$-type oxides, it is still much less than the applied criterion. Combining the experimental data and the dynamical mean field theory, we demonstrate that a $ZT$ value larger than one in electron-doped $CaMnO_3$ systems seems rather unlikely, so searching good thermoelectric oxides in electron-doped manganites may be inadvisible. Some approaches in looking for new TE materials among transition metal oxides are recommended. New TE oxides with high performance are most possible in such systems with merits as follows: large electronic effective mass, strong correlation of electrons, complex spin/orbital state, narrow energy band, low ordering temperature, or frustration.

**Acknowledgment.** The authors acknowledge financial support of the National Natural Science Foundation of China (Grants 50672019 and 10804024).

**Supporting Information Available:** Detailed density data and SEM micrographs of selected samples. This material is available free of charge via the Internet at http://pubs.acs.org.